

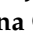



## Article

# Effect of Acyl Chain Length on Hydrophobized Cashew Gum Self-Assembling Nanoparticles: Colloidal Properties and Amphotericin B Delivery

Ana R. Richter<sup>1</sup>, José G. Veras-Neto<sup>1</sup>, Jeanlex S. Sousa<sup>2</sup>, Josilayne F. S. Mendes<sup>3</sup>, Raquel O. S. Fontenelle<sup>3</sup> ,  
Stéphanie A. N. M. Silva<sup>4</sup> , José D. B. Marinho-Filho<sup>4</sup>, Ana J. Araújo<sup>4</sup>, Judith P. A. Feitosa<sup>1</sup>,  
Haroldo C. B. Paula<sup>1</sup>, Francisco M. Goycoolea<sup>5</sup>  and Regina C. M. de Paula<sup>1,\*</sup> 

<sup>1</sup> Department of Organic and Inorganic Chemistry, Federal University of Ceará, Fortaleza 60455-760, Brazil

<sup>2</sup> Department of Physics, Federal University of Ceará, Fortaleza 60455-760, Brazil

<sup>3</sup> Biological Sciences Course, State University of Vale of Acaraú, Sobral 62040-370, Brazil

<sup>4</sup> Cell Culture Laboratory of the Delta, LCC Delta, Parnaíba Delta Federal University (UFDPAr), Parnaíba 64202-020, Brazil

<sup>5</sup> School of Food Science and Nutrition, University of Leeds, Leeds LS16 7PA, UK

\* Correspondence: rpaula@dqoi.ufc.br



**Citation:** Richter, A.R.; Veras-Neto, J.G.; Sousa, J.S.; Mendes, J.F.S.; Fontenelle, R.O.S.; Silva, S.A.N.M.; Marinho-Filho, J.D.B.; Araújo, A.J.; Feitosa, J.P.A.; Paula, H.C.B.; et al. Effect of Acyl Chain Length on Hydrophobized Cashew Gum Self-Assembling Nanoparticles: Colloidal Properties and Amphotericin B Delivery. *Colloids Interfaces* **2022**, *6*, 65. <https://doi.org/10.3390/colloids6040065>

Received: 20 September 2022

Accepted: 2 November 2022

Published: 4 November 2022

**Publisher's Note:** MDPI stays neutral with regard to jurisdictional claims in published maps and institutional affiliations.



**Copyright:** © 2022 by the authors. Licensee MDPI, Basel, Switzerland. This article is an open access article distributed under the terms and conditions of the Creative Commons Attribution (CC BY) license (<https://creativecommons.org/licenses/by/4.0/>).

**Abstract:** Given its many potential applications, cashew gum hydrophobic derivatives have gained increasing attraction in recent years. We report here the effect of acyl chain length on hydrophobized cashew gum derivatives, using acetic, propionic, and butyric anhydrides on self-assembly nanoparticle properties and amphotericin B delivery. Nanoparticles with unimodal particle size distribution, highly negative zeta potential, and low PDI were produced. Butyrate cashew gum nanoparticles presented smaller size ( $\sim 100$  nm) than acetylated and propionate cashew gum nanoparticles and no cytotoxicity in murine fibroblast cells was observed up to  $100 \mu\text{g/mL}$  for loaded and unloaded nanoparticles. As a proof of concept of the potential use of the developed nanoparticle as a drug carrier formulation, amphotericin B (AmB) was encapsulated and fully characterized in their physicochemical, AmB association and release, stability, and biological aspects. They exhibited average hydrodynamic diameter lower than  $\sim 200$  nm, high AmB efficiency encapsulations (up to 94.9%), and controlled release. A decrease in AmB release with the increasing of the anhydride chain length was observed, which explains the differences in antifungal activity against *Candida albicans* strains. An excellent storage colloidal stability was observed for unloaded and loaded AmB without use of surfactant. Considering the AmB delivery, the acyl derivative with low chain length is shown to be the best one, as it has high drug loading and AmB release, as well as low minimum inhibitory concentration against *Candida albicans* strains.

**Keywords:** acylated derivatives; nanoparticles; amphotericin B; colloidal stability

## 1. Introduction

Fungal and bacterial borne diseases have increased and become a global health problem [1,2] and the clinical treatment of systemic fungal diseases is, therefore, a major challenge.

Amphotericin B (AmB) is a second-line antifungal used against most systemic fungal infections. Since the 1960s, it has been used for the clinical treatment of early fungal diseases and, several years later, also for leishmaniasis [3]. The drug is highly active, but its clinical use is limited due to the frequent toxicity reported in the parenteral administration of the conventional formulations, composed of AmB micelles and sodium deoxycholate [4]. Given the great difficulties of working with AmB, nanotechnology approaches have been adopted in the creation of AmB carriers. A growing number of recent research in the field of nanotechnology on amphotericin B carrier systems have resulted in many improvements such as augmented bioavailability, and decreased hemo- and cytotoxicities [1,2,5–8].

Self-assembled nanoparticles have been proposed as drug carriers as they form stable structure without the need of using chemical crosslinking agents [9]. The formation of this kind of nanoparticle stems from the presence of amphiphilic groups in a polymeric macromolecule which self-assemble into a shell-core structure capable of encapsulating hydrophobic drugs [10–12].

Several polysaccharides, such as dextran, chitosan, and pullulan, have been chemically modified to improve their physicochemical, mechanical, or biological properties, expanding their range of applications as new materials. Among the polysaccharides, cashew gum and its derivatives have attracted much attention in recent years owing to their potential application.

Cashew gum obtained from Brazilian exudate is a heteropolysaccharide, previously characterized as composed mainly of galactose, glucose, arabinose, rhamnose, and glucuronic acid [13,14]. Menestrina et al. [14] also found a small amount of mannose. The polysaccharide has a branched galactan main core linked by (1→3), (1→6), and (1→3, 6) bonds, whereas the other monosaccharides are in the side chains [13,14]. Due to its versatility and biocompatibility, cashew gum has been proposed for biomedical applications [15–17].

In order to produce a self-assembling based nanocarrier, most polysaccharides need to be derivatized by introducing hydrophobic functions. Usually, insertion of hydrophobic groups can be achieved by O-acetylation with acetic anhydride [18–21]. Nanoparticles of cashew gum modified with acetic anhydride were proposed to encapsulate indomethacin [22], diclofenac [23], amphotericin B [24], and epiisopiloturine [25]. These NPs were also tested as insulin delivery systems after polyelectrolyte complexation with chitosan [26]. Other hydrophobic modifications of cashew gum with alkenyl succinic anhydride [27] and phthalate anhydride [28] were also investigated. Although several investigations have been carried out using anhydride to modify cashew gum, as mentioned above, no reports on the investigation of the acyl chain length on self-assembling nanoparticle properties and amphotericin B delivery were found.

The aim of this work was to investigate the effect of acyl groups' chain length in derivatized cashew gum on particle size, storage colloidal stability, encapsulation, and release of AmB. To this purpose two new acylated derivatives were produced with propionic and butyric anhydrides and, for comparison with previous published results, acetylated cashew gum was also produced in the same reaction condition of the new derivatives. Hence, this study may highlight the effect of acyl groups size on the production of stable nanoparticles of polysaccharide obtained from cashew tree exudate with potential application in drug delivery of hydrophobic drugs.

## 2. Materials and Methods

### 2.1. Materials

Cashew (*Anacardium occidentale*) gum exudate was donated by EMBRAPA (Empresa Brasileira de Pesquisa Agropecuária, Fortaleza City, Brazil) and the cashew gum (CG) was isolated and purified according to the protocol previously developed by our group [29] using precipitation with ethanol. CG was acylated with three different anhydrides (acetic, propionic, and butyric). Anhydrides were purchase from VETEC (São Paulo, Brazil), pyridine from Sigma Aldrich (São Paulo, Brazil), and dimethylsulfoxide from Synth (São Paulo, Brazil). Amphotericin B (AmB) was purchased from Ethycol (Fortaleza, Brazil). All reagents were used without further purification.

The CG used in this study has an average molar mass of  $6.9 \times 10^4$  g/mol as determined by size exclusion chromatography using refractive index detector and the molar sugar ratio for galactose:glucose:arabinose:rhamnose:glucuronic acid was determined as being equal to 1.00:0.20:0.08:0.05:0.06.

### 2.2. Synthesis of Acylated Cashew Gum

CG was acylated as previously reported by Motozato et al. [30], with some modifications. Briefly, CG (1 g) was suspended in 20 mL of formamide for 1 h at 50 °C. Pyridine and the respective anhydride were added to the flask (gum:pyridine:anhydride molar ratio was

fixed in 1:6:9) and the reaction was kept under stirring for 24 h, in the temperature range of 50–55 °C. The products were precipitated in 400 mL of distilled water, filtered, washed with water, and dried in hot air. Cashew gum modified with acetic, propionic, and butyric anhydrides were denominated CGAc, CGProp, and CGBut, respectively.

### 2.3. FT-IR Spectroscopy

The Fourier transform IR spectra (FT-IR) were recorded with a Shimadzu IR 8300 between 400 and 4000  $\text{cm}^{-1}$ . The samples were analyzed using KBr pellet.

### 2.4. Nuclear Magnetic Resonance

Using a Fourier transform Bruker Advance DRX 500 spectrometer with an inverse multi-nuclear gradient probe-head equipped with z-shielded gradient coils and a Silicon Graphics workstation,  $^1\text{H}$  NMR (500 MHz) spectra in deuterated DMSO were recorded at 80 °C.

### 2.5. Acyl Content and Degree of Substitution (DS)

Acyl content and degree of substitution were determined by titration method described by Sánchez-Rivera et al. [31]. Acylated cashew gum (300 mg) was placed in a flask and 75% ethanol (12 mL) was added. The solution was stirred for 30 min at 50 °C. NaOH 0.503 mol/L (12 mL) was added and heated for an additional 15 min. The flask was sealed and allowed to stand for 72 h at room temperature. Subsequently, the amount of unconsumed NaOH was determined by titration with hydrochloric acid, using phenolphthalein as indicator. Determination of the acyl group mass percentage was calculated with the equation described by Garg and Jana [32]:

$$AG (\%) = \frac{(V_1 - V_2) \times M_1 \times M_2 \times 10^{-3}}{w} \times 100 \quad (1)$$

where  $AG (\%)$  is the acyl group percentage,  $V_1$  is the HCl volume used to titrate the blank (mL),  $V_2$  is the HCl volume used to titrate the sample (mL),  $M_1$  is the molarity of HCl (0.505 mol/L), and  $w$  is the sample mass. When the acyl group is acetyl,  $M_2 = 43$  g/mol, when it is propionyl,  $M_2 = 57$  g/mol, and when it is butyryl,  $M_2 = 71$  g/mol.

$DS$  indicates the average number of hydroxyl groups substituted by acyl groups (acetyl, propionyl, or butyryl groups) per monosaccharide unit, and was calculated as described by Garg and Jana [32];

$$DS = \frac{162 \times AG}{M_2 \times 100 - [(M_2 - 1) \times AG]} \quad (2)$$

when  $AG$  is the acyl group percentage and  $M_2$  is the acyl group molar mass. When  $M_2$  is acetyl,  $M_2 = 43$  g/mol, when it is propionyl,  $M_2 = 57$  g/mol, and when it is butyryl,  $M_2 = 71$  g/mol.

### 2.6. Preparation of Cashew Gum Acylated Nanoparticles

Self-assembled nanoparticles were prepared by the dialysis method. Ten milligrams of acylated cashew gum were dissolved in 10 mL of DMSO. The solution was dialyzed against distilled water using a dialysis membrane ( $M_w$  cut off 14,000 g/mol) for 3 days. The nanoparticles were frozen and stored until characterization. The final concentration of the nanoparticle solutions was 0.4 mg/mL, for all systems.

### 2.7. Amphotericin B Encapsulation

AmB was encapsulated into the nanoparticles, using the same preparation procedure as described above, however the drug was previously dissolved in DMSO and added to acylated cashew gum derivative solution, and dialyzed for 72 h against distilled water in a light-protected vessel.

For determination of the encapsulation efficiency ( $EE\%$ ), nanoparticles were frozen and freeze dried. The material in powder form was resuspended in DMSO and centrifuged

at  $40,000 \times g$  for 0.5 h. By doing so, the nanoparticle matrix cracked and released the encapsulated drug. After centrifugation, the AmB concentration was determined using a spectrophotometer UV-Vis (Shimadzu UV-1800) at  $\lambda = 391$  nm against a suitable calibration curve in DMSO:

$$A = 0.00238 + 78.5352c \quad (3)$$

where  $A$  is the absorbance and  $c$  is the AmB concentration in mg/mL.

The encapsulation efficiency ( $EE\%$ ) was calculated from the following equation:

$$EE(\%) = \frac{w_1}{w_2} \times 100 \quad (4)$$

where  $w_1$  is the mass of AmB in nanoparticles and  $w_2$  is the mass of AmB added.

The loading capacity ( $LC$ ) was determined by following equation:

$$LC(\%) = \frac{w_1}{w} \times 100 \quad (5)$$

where  $w_1$  is the mass of AmB loaded and  $w$  is the nanoparticle mass. The experiment was carried out in triplicate.

### 2.8. Dynamic Light Scattering

A Nanosizer ZS 3600 system (Malvern Instruments Ltd., Worcestershire, UK) was used for particle size and zeta potential determinations. The particle size distributions and polydispersity index (PDI) of the acylated cashew gum nanoparticles were obtained by dynamic light scattering with non-invasive back scattering (DLS-NIBS) at  $25^\circ\text{C}$  upon irradiation of the sample using a 4-mW helium/neon red laser ( $\lambda = 633$  nm). The detection was carried out at an angle of  $173^\circ$ . Non-negative least-squares (NNLS) or CONTIN algorithms were used for data analysis [33]. The Zetasizer equipment software was used to extract the decay times and determine the diffusion coefficient ( $D$ ). The average hydrodynamic radii ( $R$ ) was obtained from the Stokes–Einstein equation  $R = K_B \cdot T / 6\pi\eta D$ , where  $D$  was obtained from the NNLS data,  $k_B$  is the Boltzmann constant,  $T$  is the absolute temperature, and  $\eta$  is the solvent viscosity [33].

The electrophoretic mobility ( $\mu$ ) of nanoparticles was measured by mixed laser Doppler velocimetry and phase analysis light scattering (M3–PALS). The Smoluchowski relation equation was used to calculate the zeta potential ( $\xi$ ):  $\xi = \mu\eta/\epsilon$ , where  $\epsilon$  is the permittivity of the solvent and  $\mu$  is the average electrophoretic mobility [33].

The measurements were performed in triplicate without sample dilution or filtration. All the measurements were made after the dialysis process, without previous lyophilization. The nanoparticle concentration was  $0.4$  mg/mL and it was confirmed by freeze drying an aliquot of the dialyzed solution and determining the mass.

### 2.9. Morphology

Nanoparticles were analyzed using Asylum MFP3D-Bio microscopy (AFM). The images were taken in tapping mode, using an EconoLTESP with nominal spring constant of  $5$  N/m and resonance frequency of  $138$  kHz. Images were acquired in intermittent contact mode (tapping mode). A volume of  $10$   $\mu\text{L}$  of diluted samples ( $1:200$  v/v) was spread onto freshly cleaned mica and vacuum dried.

### 2.10. State of AmB Aggregation

To determine the state of aggregation of AmB in nanoparticles before extraction, the nanoparticles with and without (blank) drug were diluted in deionized water and the UV/Vis (Shimadzu UV-1800) spectrum was registered. The experiment was also performed with a commercial Sigma AmB solution (with sodium deoxycholate). The state of AmB aggregation was determined using the methodology proposed by Barwicz, Christian, and Gruda [34]. The ratio of absorbances at  $\sim 345$  (peak I) and  $406$  nm (peak IV) ( $A_I/A_{IV}$ ) in

the AmB UV/Vis spectrum, were used to indicate the AmB aggregation pattern. AmB in monomeric forms usually has an  $A_I/A_{IV}$  ratio around 0.3 or lower, while an  $A_I/A_{IV}$  ratio higher than 2 indicates AmB aggregation [33]. Each experiment was performed in triplicate.

#### 2.11. Storage Stability

The storage stability was ascertained by measuring the size distribution and the particle size of nanoparticles every month for three years for unloaded nanoparticles and two years for AmB-loaded nanoparticles. Nanoparticle solution concentrations of 0.4 mg/mL were kept refrigerated at  $4 \pm 2$  °C. Measurements were made in triplicate from nanoparticle solutions without prior dilution or filtration processing. Each experiment was performed in triplicate.

#### 2.12. In Vitro Drug Release

The release profiles of the AmB-loaded nanoparticles were obtained using a dialysis system. Each sample (10 mg) was introduced into cellulose acetate membranes (MW cut off 14,000 g/mol) and dialyzed against 20 mL of PBS buffer solution containing 0.25% sodium lauryl sulfate, at pH 7.4, and 37 °C for 72 h. Aliquots were taken at fixed time intervals and analyzed by spectrophotometry in the UV/Vis region (Shimadzu UV-1800). Absorbance measurements ( $\lambda = 368$  nm) were converted into the percentage of drug released, according to a previously established AmB calibration curve in PBS buffer solution containing 0.25% sodium lauryl sulfate ( $R^2 = 0.999$ ).

$$A = 0.00175 + 53.8163 c \quad (6)$$

where  $A$  is the absorbance and  $c$  is AmB concentration. Each experiment was performed in triplicate.

#### 2.13. In Vitro Antifungal Assay—Broth Microdilution Method

The minimum inhibitory concentrations (MIC) for blank and AmB-loaded acylated nanoparticle and the Sigma-Aldrich AmB solution were determined via the broth micro dilution method using 96-well plates according to document M27-A3, from the Clinical and Laboratory Standards Institute-CLSI (formerly NCCLS) [35]. Stock solutions of nanoparticles (64  $\mu\text{g/mL}$ ) in sodium lauryl sulfate (0.150 mL) were serially diluted to the range of 0.007–16  $\mu\text{g/mL}$  in RPMI 1640 medium. AmB (0.007–16  $\mu\text{g/mL}$ ) was used as a standard. Control experiments on non-treated cells was also carried out. The microplates were incubated at 35 °C and fungal growth/inhibition was observed after 48 h. The MIC was defined as the lowest concentration of an antimicrobial agent that prevents visible growth of a microorganism. The results were read visually as recommended by the CLSI (Clinical and Laboratory Standards Institute, 2008). Five *Candida albicans* strains were used in the experiment, one was obtained from the American Type Culture Collection (ATCC 90028), three clinical isolates of *C. albicans* (LABMIC 0103, LABMIC 0104, LABMIC 0105) from the Santa Casa de Misericórdia Hospital (Sobral, Ceará, Brazil), and one clinical isolate (LABMIC 0106) obtained from the Heart Hospital (Sobral, Ceará, Brazil). Each experiment was performed in duplicate.

#### 2.14. Cytotoxicity Assay

The cytotoxic effect of CGAc, CGProp, CGBut (unloaded vectors), CGAc AmB, CGProp AmB, and CGBut AmB (loaded vectors), was determined by MTT assay, according to Mosmann [36]. L929 cells were seeded in 96-well plates at the concentration of  $1 \times 10^5$  cell/mL. After 24 h of growth, cells were treated at 25  $\mu\text{g/mL}$ , 50  $\mu\text{g/mL}$ , and 100  $\mu\text{g/mL}$  of tested samples as a negative control (C-) and then incubated at 37 °C for 69 h. Amphotericin B at concentration of 100  $\mu\text{g/mL}$  in serial dilution of ratio 2 was used as a positive control. MTT solution (0.5 mg/mL) was added to each well and incubated for 3 h. At the end of the incubation period, MTT formazan product was dissolved in DMSO, and cell viability was

quantified using a multi-wall microplate reader (Molecular Devices, Spectramax 190) at 595 nm and growth inhibition was estimated.

### 2.15. Statistical Analysis

Statistical analysis was carried out using GraphPad Prism version 9.2.0 for Windows, (GraphPad Software, San Diego, CA, USA, [www.graphpad.com](http://www.graphpad.com) (accessed on 28 October 2022)). All biophysical and stability experiments were conducted in triplicate, excepting biological experiments that were performed in duplicate. Values were expressed as mean  $\pm$  SD. Comparison analysis was performed between tests and control. Statistical differences were evaluated using one-way analysis of variance (ANOVA).

## 3. Results and Discussion

### 3.1. Acylated Cashew Gum

Modified cashew gum was prepared by addition of three anhydrides (acetic, propionic, and butyric) in the same CG:anhydride molar ratio (1:9) and were designated CGAc, CGProp, and CGBut, respectively. As can be seen in Table 1, the modified cashew gum derivatives showed an increase in acyl group mass percentage and in yield with increasing of anhydride chain length (from acetyl to butyl groups). The increase in acyl group percentage is expected as the same molar ratio of polysaccharide and acyl anhydride was used in the synthesis and the molar mass of acyl group increase with increasing of chain length. A similar result was observed in our previous studies for the acylation of *Sterculia striata* polysaccharide with acetic and propionic anhydrides [37,38].

**Table 1.** Effect of anhydride on the degree of substitution (DS) and yield.

Sample	% acyl Groups	DS	Yield (%)
CGAc	30.7 $\pm$ 0.9	1.65 $\pm$ 0.07	49.1 $\pm$ 5.1
CGProp	33.6 $\pm$ 3.7	1.29 $\pm$ 0.19	53.1 $\pm$ 3.9
CGBut	41.2 $\pm$ 1.3	1.12 $\pm$ 0.10	65.9 $\pm$ 3.5

It is observed that increase in anhydride chain length led to a decrease in the substitution degree, an effect that may be justified as being the consequence of steric hindrance with an increase in anhydride chain. Garg and Jana [32] acylated starch with the acetic, propionic, and butyric anhydride and the DS was reported to be dependent on anhydride chain length [32]. Butylated starch had a low DS, compared to acetylated and propionate starch, at the same condition [32], this is in good agreement to our data.

### 3.2. FTIR Analysis

FTIR spectra for CG and acylated CG are shown in Figure 1. The CG spectrum shows a broad band centered at 3394  $\text{cm}^{-1}$ , due to O-H stretching vibrations; 2926  $\text{cm}^{-1}$  attributed to C-H stretching vibrations; 1634  $\text{cm}^{-1}$  due to the O-H scissor vibrations of bonded water molecules; and 1145, 1086, and 1033  $\text{cm}^{-1}$  assigned to stretching vibrations of C-O-C from glycosidic bonds and the bending of O-H from alcohols. Altogether, these bands are characteristic of the fingerprint of polysaccharide structures [39,40].

A new band around 1750  $\text{cm}^{-1}$  due to C=O vibration of the ester linkage appeared in all remaining spectra (B, C, and D), as clear evidence of the success of acylation reactions, in good keeping with other works [22,24,32,37,38]. Moreover, the deformation  $\text{CH}_3$  vibration at 1360  $\text{cm}^{-1}$  is observed in all three derivatives as well as increases in bands in the range of 2950–2850  $\text{cm}^{-1}$ , corresponding to the stretching of CH of the methyl and methylene groups in acyl derivatives (see Figure S1), are observed for CGProp and CGBut derivatives. Other bands characteristic of CG polysaccharide (e.g., 3379, 1150, 1080, 1030  $\text{cm}^{-1}$ ) are also present [22,24,32,37,38].

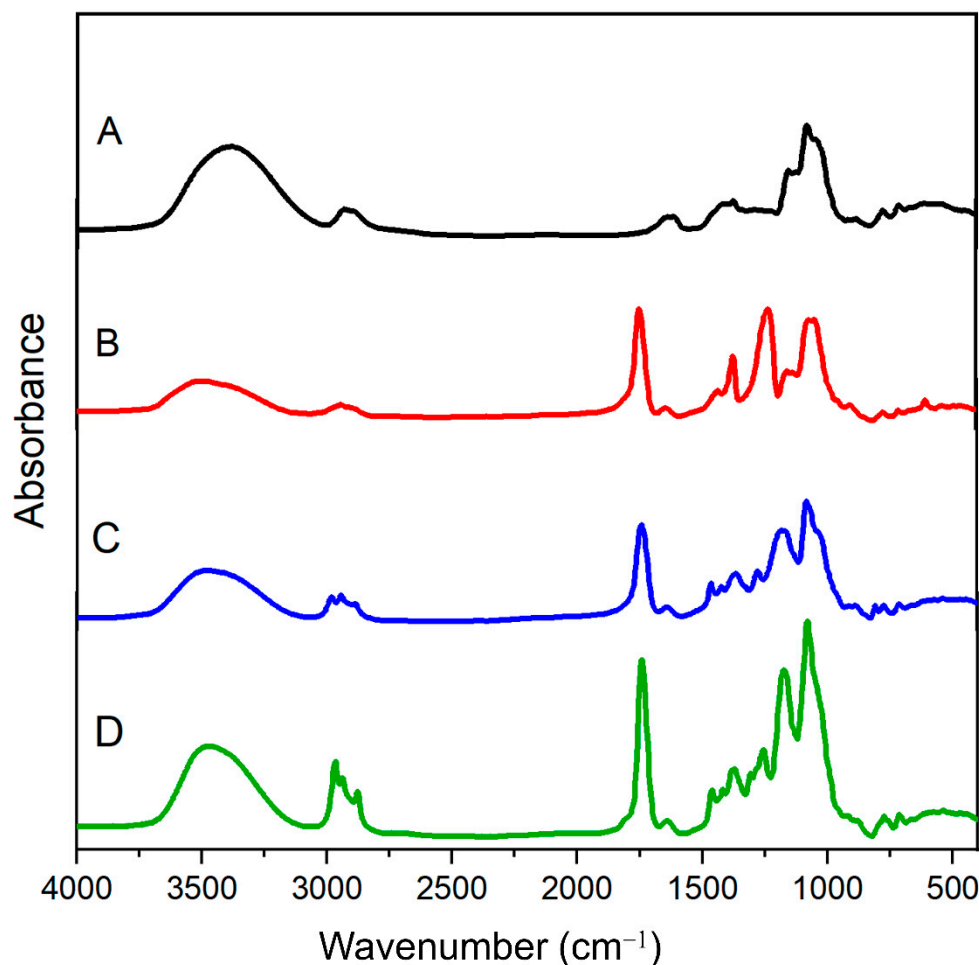


**Figure 1.** FTIR spectra for cashew gum and acylated derivatives: (A) CG; (B) CGAc; (C) CGProp; (D) CGBut.

### 3.3. NMR Spectroscopy

In Figure 2 the  $^1\text{H}$  NMR spectra for CG and acylated CG samples can be seen. The  $^1\text{H}$  NMR spectrum for cashew gum without modification (Figure 2A) presented characteristic anomeric protons in the region of 4.4–5.0 ppm [41]. The signals in this region are assigned to  $\alpha$ -D-glucose (4.95 ppm),  $\alpha$ -L-rhamnose (4.81 ppm),  $\beta$ -D-galactose (1 $\rightarrow$ 3) (4.69 and 4.43 ppm), and  $\beta$ -D-glucuronic acid (4.51 ppm). H-2–H-5 signals are overlapped in the regions of 3.4–4.3 ppm. A quartet signal in the region of 1.26 ppm is due to the methyl protons of rhamnose [41].

It is possible to observe, in the acylated derivatives (B, C, and D), the appearance of new signals in the region of 1.06–2.3 ppm. The signal in the region of 1.8–2.2 ppm is due to hydrogen in the methyl group of CGAc (Figure 2B) [22,24,42]. For CGProp, the signals (Figure 2C) in 2.3 and 1.06 ppm are due to hydrogen in the methylene and methyl, respectively, of the ethyl group of propionyl [43]. The CGBut derivative shows three signals (Figure 2D) due to two methylene groups (2.28 and 1.57 ppm) and one methyl group (0.9 ppm) of butyrate in the derivative [44]. The NMR data corroborate the presence of new bands assigned to CO carbonyl present in the FTIR spectra of the acylated derivatives. The signal at 2.5 ppm is due to DMSO used as solvent.

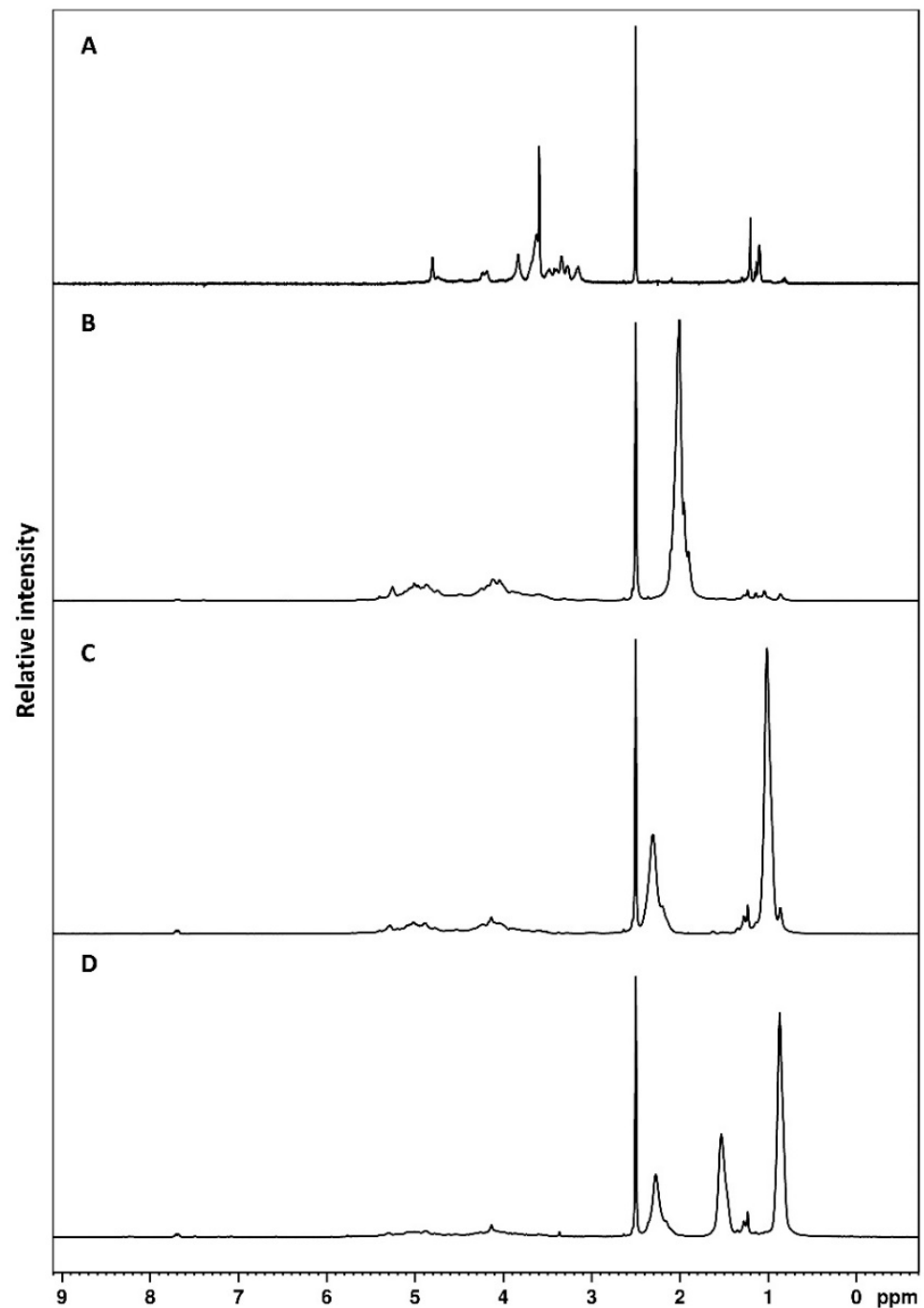


**Figure 2.**  $^1\text{H}$  NMR (500 MHz) spectra for CG (A), CGAc (B), CGProp (C), and CGBut (D) derivatives in  $\text{DMSO-d}_6$ .

### 3.4. Characterization of Nanoparticles

Given that the cashew gum modified with acetic anhydride is hydrophobic and capable of self-organizing into micelles forming nanoparticles [22–24], the dialysis method was used to prepare the self-assembled nanoparticles. The hydrodynamic diameter, in an aqueous medium, was determined by DLS at 25 °C. Figure 3 shows the values of particle size, PDI, and zeta potential ( $\zeta$ ) for acylated cashew gum nanoparticles. All the systems show unimodal size distributions without evidence of aggregation (Figure 4E,F).



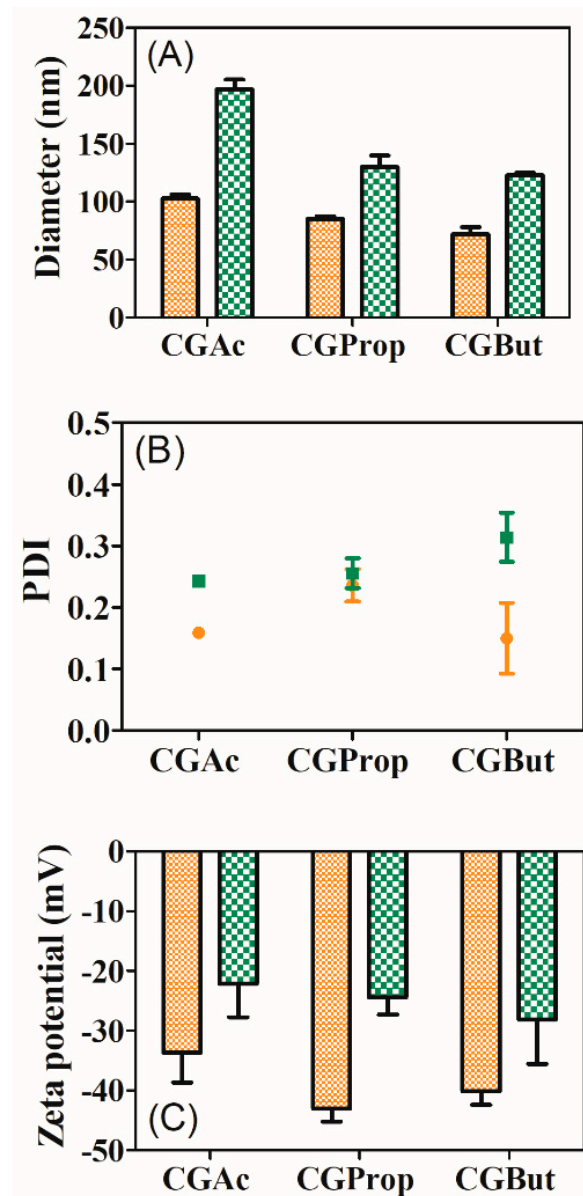


**Figure 3.** Hydrodynamic diameter (A), PDI (B), and zeta potential (C) for unloaded and AmB-loaded nanoparticles. Unloaded nanoparticles (orange) and AmB-loaded nanoparticles (green).

Particle diameters for the unloaded nanoparticles were  $103 \pm 4$ ;  $85 \pm 2$ , and  $72 \pm 6$  nm for CGAc, CGProp, and CGBut nanoparticles, respectively (Figure 3A). A decrease in particle size with increasing of anhydride chain length was observed, a fact that may be due to the higher interaction among the hydrophobic polysaccharide chains, which led to the observed decrease in particle size. Particle sizes were found to be smaller for acylated nanoparticles in comparison to unmodified gum ( $225 \pm 22$  nm).

The PDI values were less than 0.3 for all systems and an increasing trend is observed only for CGAc and CGProp ( $0.159 \pm 0.001$  and  $0.236 \pm 0.026$ , respectively). The CGBut nanoparticle has a lower PDI value ( $0.149 \pm 0.057$ ). The  $\zeta$ -potential values for these systems were all negative and the mean  $\zeta$  values ( $-30$  to  $-40$  mV) for all nanoparticles indicate stable systems [45,46]. The greater the  $\zeta$ -potential, in modulus, the more likely the suspension is to be stable, because the charged particles repel each other electrostatically and hence this force overcomes the natural tendency to aggregate a feature of all stable systems. A lower value for  $\zeta$ -potential, in modulus, is observed for unmodified cashew gum solution ( $-20$  mV).

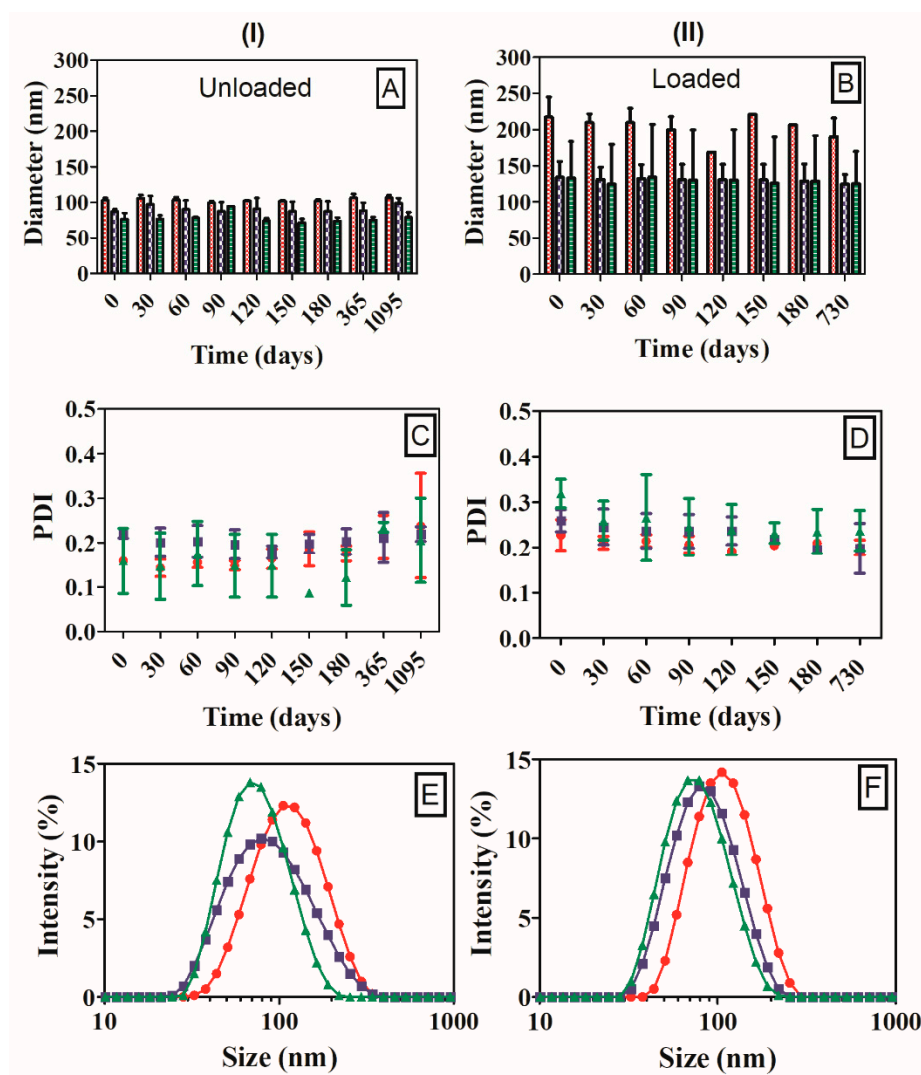


**Figure 4.** Storage stability and particle size distribution for unloaded and AmB-loaded acylated nanoparticles in aqueous solution at 4 °C. CGAc (red), CGProp (blue), and CGBut (green). Unloaded nanoparticles: Particle size (A), PDI (C) and size distribution (E); AmB loaded nanoparticles: Particle size (B), PDI (D) and size distribution (F), as a function of time.

Dias et al. [23] and Pitombeira et al. [22] reported on cashew acetylated with acetic anhydride and described nanoparticles produced via self-organization in a dialysis system using acetone and DMSO solvents, respectively. The degree of substitution was 2.8 for both systems. Particle sizes were significantly higher using acetone ( $302.0 \pm 0.9$  nm) [23] and DMSO (179 nm) [22]. Lima et al. [24] showed that depending on reaction conditions, particles with a size suitable for delivery systems ( $< \sim 250$  nm) can be obtained from acetylated cashew gum with acetic anhydride. Phthalate cashew gum nanoparticles show particle sizes of 288 nm [28]. The nanoparticles obtained in this work show smaller particle size than other previously acylated cashew gum derivatives [22,23,28].

The effect of AmB incorporation on particle size,  $\zeta$ -potential, and polydispersity of CGAc, CGProp, and CGBut was also investigated. The particle size and the polydispersity of loaded nanoparticles is higher than the unloaded systems (Figure 3),  $193 \pm 8$  nm and 0.222 for AmB-loaded CGAc,  $136 \pm 4$  nm and 0.255 for AmB-loaded CGProp, and  $123 \pm 2$  nm and 0.314 for AmB-loaded CGBut. This is probably due to electrostatic interactions of the drug with the polymer chain that occur during the encapsulation process [47]. The same behavior was reported by Sombra et al. [37] for AmB loaded in nanocapsules of *Sterculia striata* polysaccharide.

$\zeta$ -potential values for loaded nanoparticles are smaller than those observed for the unloaded nanoparticles. No significant difference in the  $\zeta$ -potential values was observed for the loaded nanoparticles ( $-22.1 \pm 5.5$  mV for AmB-loaded CGAc,  $-24.4 \pm 2.8$  mV for AmB-loaded CGProp, and  $-28.1 \pm 7.4$  mV for AmB-loaded CGBut). There are significant differences of  $\zeta$ -potential for loaded and unloaded nanoparticles (Figure 3C), where a decrease, in modulus, is observed for loaded nanoparticles. Adsorption of oppositely charged patches on nanoparticle surfaces may be responsible for the decrease in  $\xi$ -potential, which can lead to system aggregation [48–50].

Encapsulation of AmB in the acylated cashew gum derivatives by self-assembling assumes that the hydrophobic part of the derivative, as well as the drug, are in the inner core of the nanoparticles, while the hydrophilic groups of derivatives are in the nanoparticle surfaces, promoting the dispersion of the system in aqueous systems. The decrease in  $\xi$ -potential observed for loaded derivatives indicates the formation of adsorbed AmB, patches, on nanoparticles surfaces, as observed for adsorption of lysozyme in Au nanoparticles [48]. As a decrease in  $\zeta$ -potential could affect the colloidal stability of loaded nanoparticles, the discussion of this relation will be done in Section 3.5.

### 3.5. Colloidal Storage Stability of Nanoparticles

To evaluate the colloidal stability of blank and AmB-loaded nanoparticles in aqueous solution under refrigeration ( $4 \pm 2$  °C), particle size, polydispersity index, and size distribution were monitored over time (Figure 4). The nanoparticles remained stable throughout the experiment, with unimodal particle size distributions, and without evidence of aggregation after three and two years, for unloaded and loaded systems, respectively.

Unloaded nanoparticles exhibit sizes under 150 nm (Figure 4A), with no significant difference ( $p < 0.05$ ) in the particle size after three years ( $107 \pm 4$  nm for CGAc,  $99 \pm 7$  nm for CGProp, and  $79 \pm 7$  nm for CGBut) compared with fresh nanoparticles ( $103 \pm 4$  nm for CGAc,  $85 \pm 2$  nm for CGProp, and  $72 \pm 6$  nm for CGBut). The loaded nanoparticles have sizes under 250 nm and the same behavior was observed without major changes (Figure 4B). The incorporation of AmB into the nanoparticles did not significantly affect the particle size after two years of storage ( $190 \pm 26$  nm for AmB-loaded CGAc,  $132 \pm 5$  nm for AmB-loaded CGProp, and  $146 \pm 37$  nm for AmB-loaded CGBut) compared with freshly loaded nanoparticles ( $193 \pm 8$  nm,  $136 \pm 4$  nm, and  $123 \pm 2$  nm for AmB-loaded CGAc, CGProp, and CGBut, respectively). For both unloaded and AmB-loaded nanoparticles, the polydispersity index values remained under 0.4 for all storage times (Figure 4C,D). These features are highly desirable, as colloidal stability was achieved without addition of surfactants.

A decrease, in modulus, in  $\zeta$ -potential has been observed for loaded nanoparticles, however no aggregation was detected in the storage stability up to two years (Figure 4B). For colloidal systems,  $\zeta$ -potential higher than  $\pm 30$  mV is considered stable for drug delivery systems [45,46], but even systems with lower  $\zeta$ -potential show stable nanoparticles such as pegylated nanoparticles [51]; this phenomenon has been explained using the DLVO theory, applied to colloidal stability. The DLVO theory suggests that stability depends not only on electrostatic repulsive forces, such as  $\zeta$ -potential, but also on van der Waals forces [46,52].

Brasili et al. [48] showed that as the amount of lysozyme increases on Au nanoparticles, above a threshold value, an increase in hydrodynamic diameter and concomitant decrease, in modulus, in  $\xi$ -potential is observed leading to aggregation. AmB-loaded NP stability can be explained by taking into account that even with decreasing zeta potential, the AmB patches adsorbed on nanoparticles were not enough to diminish the electrostatic repulsion, resulting in a stable system.

Similar results were observed in nanocapsules of *Sterculia striata* gum acylated with acetic anhydride [37] and propionic [38], where no significant difference was found in the size and PDI after one year of storage. Cashew gum acetylated with acetic anhydride also presents one-year size control in storage conditions [22].

### 3.6. Morphology

AFM height and amplitude images of AmB-loaded nanoparticles are shown in Figure 5. Nanoparticles with smooth surface, and smaller size than those obtained by DSL were observed. At closer inspection, the magnification of the AmB-loaded images showed homogeneous samples, without phase difference. Two possible explanations for the absence of texture in the image can be theorized. First, the increase in the acyl chain length and DS was not enough to lead to a phase difference, and second, the AmB is preferentially located only inside of nanoparticles. A different result was reported by Richter et al. [8] for self-assembly nanoparticles of CG grafted with PLA. The slight increase in DP of CG-grafted PLA and the variation of hydrophobicity leads to a difference in AFM phase images [8].

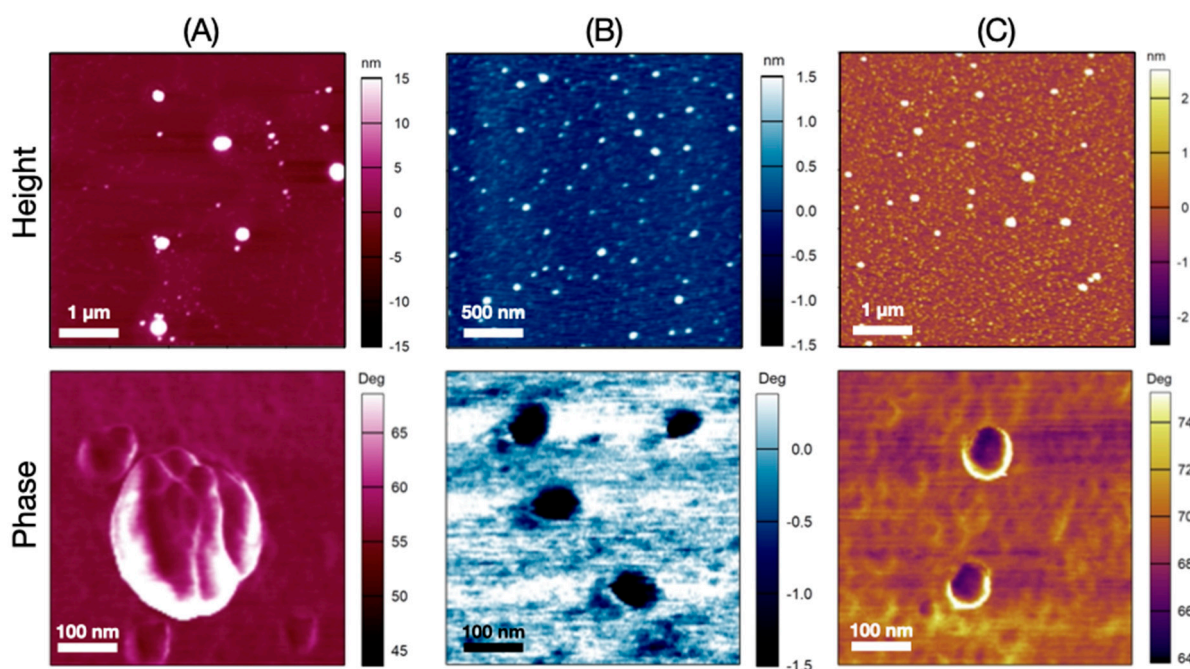


**Figure 5.** AFM images of height of: (A) CGAc AmB, (B) CGProp AmB, and (C) CGBut AmB nanoparticles.

### 3.7. Aggregated States of AmB in Acylated Nanoparticles

The UV/Vis spectrum of polyenes is sensitive to conformational changes due to aggregation. The spectral change characteristic of AmB self-aggregation can be represented by the ratio of absorbance between the first peak (I) at 348 nm and the fourth peak (IV) at 409 nm [34]. This ratio has values around 2.0 for the spectrum of the aggregated AmB species and around 0.3 for monomeric AmB [34]. Amphotericin B aggregation is reported to be related to its chronic toxicity [53–55].

The AmB UV/Vis spectrum in DMSO in Figure 6A shows four bands and AmB is in its monomeric form, as the ratio between bands at 352 and 415 nm is very small. In aqueous AmB solution, at low concentrations of AmB ( $5.0 \times 10^{-7}$  mol/L), the UV/Vis spectrum of AmB shows band patterns similar to that in DMSO; being in its monomeric form, as the concentration increases ( $5.0 \times 10^{-5}$  mol/L), the spectrum is progressively modified until a new intense band appears near 340 nm, indicating the presence of aggregate species [56].

For the commercial AmB aqueous solution (with surfactant) from Sigma-Aldrich, at a concentration of  $2 \times 10^{-5}$  mol/L (Figure 6A) an intense band at 326 nm, characteristic of aggregated AmB is observed, besides the three characteristic bands are shifted to 364, 384, and 407 nm when compared to the spectrum of the AmB in its monomeric form in DMSO.

Inspection of AmB-loaded nanoparticle UV/Vis spectra (Figure 6B) reveals that a displacement between the AmB bands was also observed, as described in the literature, but the profile remains similar. There is an intense band at 342 nm for the CGProp AmB and three other bands of lower intensity at 365, 387, and 420 nm. The spectrum for CGAc

AmB and CGBut AmB nanoparticles is very similar to CGProp NPs, with small wavelength variations, presenting bands at 330, 365, 387, and 418 nm.

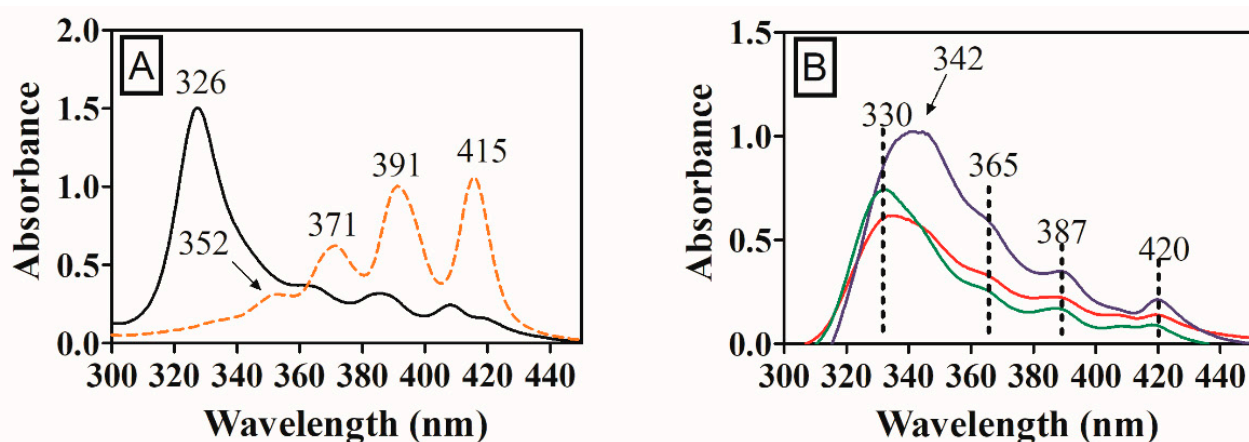


**Figure 6.** UV/Vis spectra of (A) commercial AmB (aqueous solution plus surfactant) (black line) and AmB in DMSO (orange line), and (B) AmB-loaded acylated nanoparticle aqueous solution CGAc AmB (red line); CGProp AmB (blue line); CGBut AmB (green line).

Displacements of the AmB UV/Vis spectrum were also observed for AmB-loaded propionate *Sterculia striata* polysaccharide nanocarrier [38], linolenic acid and oligochitosan micelles [57], CG-grafted PLA nanoparticles [8], and acetylated *Sterculia striata* polysaccharide nanocapsules [36].

Reported data for the ratios between AI/AIV bands for commercial formulations are discrepant. For example, for Fungizone, values of 2.9 [58], 3.7 [59], and 6.4 [55,60] have been documented. For Amphocil and Ambisone in 5% dextrose solution, ratios of AI/AIV bands were reported to be 9.1 and 4.8, respectively [58]. The commercial Sigma-Aldrich AmB solution used in this work shows an AI/AIV band ratio value of 6.1.

The AI/AIV ratios for the acylated AmB-loaded nanoparticles were 4.2 (CGAc AmB), 3.8 (CGProp AmB), and 7.1 (CGBut AmB). These values indicate that the AmB loaded in the developed nanoparticle systems occurs in aggregated state, however, the band ratio values are in the range of figures found for the commercial formulations already in use [55,58–60].

### 3.8. AmB Encapsulation and In Vitro Release

Encapsulation efficiency (EE) and loading capacity (LC) are important characteristics for nanoparticle-based drug delivery formulations and their outcomes defines the success of the therapy. Carrier systems that have higher EE exhibit a slow-release pattern, which maintains the therapeutic levels for a longer time, thus eliminating the need for more dosages and its associated toxicity [61].

The EE and LC were determined using an initial AmB concentration of 1.0 mg/mL of the nanoparticles' preparation. The values of EE and LC were, respectively,  $94.9 \pm 4.7\%$  and  $9.5 \pm 0.5\%$  for CGAc AmB,  $78.5 \pm 4.1\%$  and  $7.9 \pm 0.4\%$  for CGProp AmB, and  $88.1 \pm 5.0\%$  and  $8.8 \pm 0.5\%$  for CGBut AmB. Despite having the lowest anhydride chain length, CGAc nanoparticles have the highest EE value, and this may be due to the higher particle size of this derivative. Lima et al. [24], using acetylated cashew gum with DS of 1.68, closer to the one obtained in this work (CGAc DS = 1.65), showed a very low AmB encapsulation efficiency (36.95%). However, nanoemulsions prepared with acetylated *Sterculia striata* polysaccharide (DS = 1.68) showed an AmB encapsulation efficiency of 92.5% [37], similar to the one observed in our work. Nanoemulsions of propionate derivative of *Sterculia striata* polysaccharide (DS = 2.53) show AmB EE% ranging from 72.3 to 98.3%, depending on derivative and AmB concentration in the formulation [38].

To investigate the potential acetylated, propionate, and butyrate cashew gum nanoparticles as AmB drug delivery devices, an in vitro release experiment was carried out using

PBS buffer (pH = 7.4) with 0.25% sodium lauryl sulfate as release medium (Figure 7). The profile shows a sustained drug release, an initial burst, followed by a steady release. The maximal AmB release percentage, after 72 h, was  $42.8 \pm 6.7$ ;  $36.6 \pm 3.6$ ; and  $24.1 \pm 4.5\%$  for CGAc AmB, CGProp AmB, and CGBut AmB, respectively. A decrease in percentage release with the increase in the anhydride chain length, likely because larger chain, promotes a better interaction with the AmB, which is reflected in a minor release.

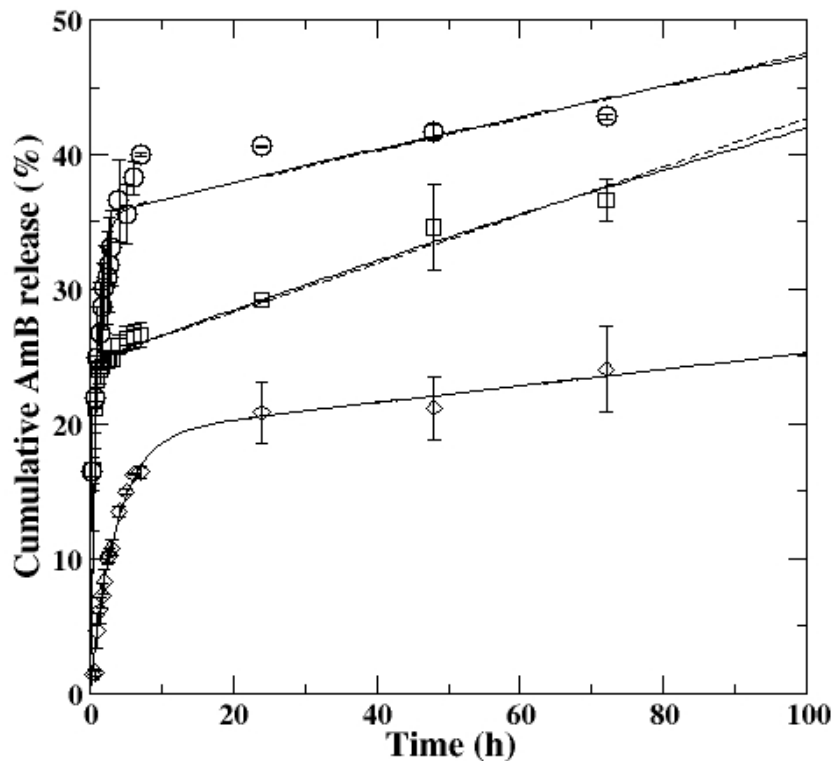


Figure 7. In vitro AmB release profile for acylated nanoparticles: CGAc AmB (○), CGProp AmB (□), CGBut AmB (◇).

Italia, Yahya, Singh, and Kumar [62] and Tiyaboonchai and Limpeanchob [59] reasoned that the rapid release of AmB in their systems was the consequence of drug molecules located in the outer nanoparticle surface during its formation process, leading to less interaction and a consequently larger facile release. A similar release profile is found for the chitosan and AmB complex, releasing approximately 21% in the first 24 h, followed by 44.5% release after 20 days of the experiment [63].

Zheng, An, and Wu [64] proposed a kinetic model that describes release systems where two mechanisms are observed as a function of time. The model assumes a second order exponential law:

$$\frac{M_t}{M_0} = \frac{k_{off}}{k_{on} + k_{off}} (1 - e^{k_s t}) + \frac{k_{on}}{k_{on} + k_{off}} (1 - e^{k_{off} t}) \tag{7}$$

where  $k_s$  is the diffusion rate,  $k_{on}$  is the drug association rate constant, and  $k_{off}$  is the drug dissociation rate constant. The model assumes that  $k_s \gg k_{on}$  and  $k_s \gg k_{off}$ .

If the  $k_s/k_{off}$  ratio is higher than 10, Equation (7) can be approximated using a linear contribution:  $1 - e^{-k_{off} t} \sim k_{off} t$  [65]:

$$\frac{M_t}{M_0} = \frac{k_{off}}{k_{on} + k_{off}} (1 - e^{k_s t}) + \frac{k_{on}k_{off}}{k_{on} + k_{off}} t \tag{8}$$

The free energy ( $\Delta G$ ) can be used to evaluate the relation between the free and bound state of the drug [64]:

$$\Delta G = -k_B T \ln \left( \frac{k_{on}}{k_{off}} \right) \quad (9)$$

where  $k_B$  is the Boltzmann's constant and  $T$  is the absolute temperature (310 K).

Fitting of Equations (7) (solid line) and (8) (dashed line) on release (Figure 7) gave very similar data for the three derivatives, thus the AmB release in acylated cashew gum derivatives has an initial burst, followed by a steady release [64,65]. The model parameters for AmB-loaded acylated cashew gum nanoparticles are shown in Table 2.

**Table 2.** Second order exponential order parameters for AmB-loaded acylated cashew gum derivative nanoparticles.

Acyl Derivatives	Model Parameters				
	$K_s$ ( $h^{-1}$ )	$K_{on}$ ( $h^{-1}$ )	$K_{off}$ ( $h^{-1}$ )	$\Delta G$ ( $10^{-21}$ J)	$R^2$
CGAc AmB	1.18	0.0037	0.0020	−2.63	0.9917
CGProp AmB	3.13	0.0080	0.0026	−4.81	0.9995
CGBut AmB	0.28	0.0037	0.0008	−6.19	0.9996

The decrease in  $\Delta G$  with increasing of acyl chain length indicates a decrease in the magnitude of the initial burst [64]. The negative values of  $\Delta G$  for all derivatives indicates a strong interaction between AmB and acyl derivatives [64].

Considering the total AmB release in 72 h, we can observe that around 70% of the AmB was released in the steady release phase for CGProp AmB, which is corroborated with higher  $K_{off}$  obtained for this derivative.

### 3.9. Cytotoxicity Assay

L929 cells, widely used in cytotoxicity tests to ensure the biocompatibility of new drugs and formulations, since it is a normal mouse cell line, was used to evaluate the toxicity of the systems present in this work. All samples tested (CGAc AmB, CGAc, CGProp AmB, CGProp, CGBut AmB, and CGBut) showed  $IC_{50}$  values above the highest concentration tested ( $>100 \mu g/mL$ ) (Figure 8), thus indicating the safety of the proposed material.

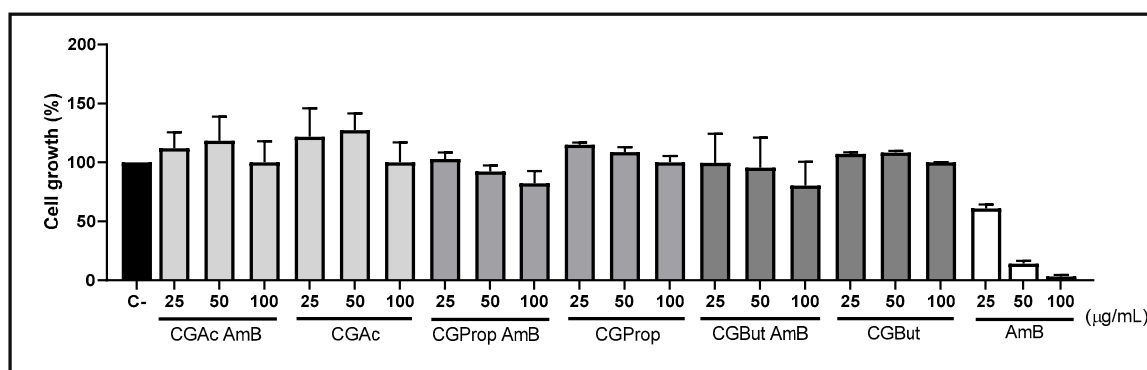


**Figure 8.** Evaluation of in vitro cell growth of CGAc AmB, CGProp AmB and GCBUT AmB (loaded vectors), CGAc, CGProp and CGBut (unloaded vectors), and Amphotericin B (AmB) after 72 h of treatment, at concentrations of 25, 50, and 100  $\mu g/mL$ .  $IC_{50}$  of Amphotericin B (positive control): 26.6  $\mu g/mL$ . C-: negative control.

Regarding the potential of free AmB, several studies demonstrate its toxicity in L929 cells. Mutlu-Agardan et al. [66] observed a decrease in cell viability from 100 to 70% at 24 h

and 48 h of 32- $\mu\text{g}/\text{mL}$  AmB treatment. Our results showed that Amphotericin B at 72 h of treatment, showed an  $\text{IC}_{50}$  value of 26.6  $\mu\text{g}/\text{mL}$ .

### 3.10. In Vitro Antifungal Test

The antifungal activity of acylated AmB-loaded nanoparticles was evaluated using five *Candida albicans* strains (Table 3). The MIC values for AmB were 1  $\mu\text{g}/\text{mL}$  for two strains and 2  $\mu\text{g}/\text{mL}$  for three strains. Similar results were reported by Sombra et al. [37] for AmB loaded in acetylated *Sterculia striata* polysaccharide. Non-treated cells show normal growth.

**Table 3.** Minimum inhibitory concentration (MIC) of AmB-loaded acylated nanoparticles against *C. albicans* strains.

Samples	MIC ( $\mu\text{g}/\text{mL}$ )				
	<i>C. albicans</i>				
	LABMIC 0103	LABMIC 0104	LABMIC 0105	LABMIC 0106	ATCC 90028
CGAc AmB	1	1	1	1	1
CGProp AmB	1	1	1	1	2
CGBut AmB	2	2	2	2	4
Free AmB	2	1	1	2	2

The AmB-loaded CGAc and CGProp nanoparticles showed the lowest values for all the strains, and the AmB-loaded CGBut nanoparticles the highest. This could be explained by the drug delivery profile. The AmB-loaded CGBut nanoparticles show a sustained drug release with maximum percentage in  $24.1 \pm 4.5\%$ , whereas AmB-loaded CGAc and CGProp were  $42.8 \pm 6.7$  and  $36.61 \pm 3.6\%$ , respectively, which justify the increase in the MIC values for AmB-loaded CGBut nanoparticles. The lowest acyl chain length derivative shows the best MIC results for all five *C. albicans* strains.

Although the MIC values for loaded acylated nanoparticles are in the same order of those observed for free AmB, the amount of drug in loaded AmB acylated nanoparticle is circa 10 times lower—see loading capacity values—thus the same efficiency in *C. albicans* strains inhibition is obtained with much lower AmB content. This finding is promising due the high nephrotoxicity of AmB.

## 4. Conclusions

Acetylated, propionate, and butyrate cashew gum derivatives were successfully synthesized. Nanoparticles prepared by self-assembly possessed particle size smaller than previously synthesized cashew gum acylated nanoparticles. Particle size decreases with increasing acyl chain length in cashew gum nanoparticle. The stability was also monitored over three years without significant variation in size. Data revealed that all AmB-loaded nanoparticles possess sizes in the range acceptable to be used in drug delivery systems and a slow-release pattern. A decrease in percentage release with the increase in the anhydride chain length was observed. Regarding the AmB delivery, the acyl derivative with low chain length CGAc showed a high drug loading and drug release profile, as well as low minimum inhibitory concentration (MIC) against all *C. albicans* strains investigated. Considering that AmB presents high nephrotoxicity, and the fact that our carrier system exhibited no cytotoxicity against murine fibroblast cells (L929), as well as satisfactory effectiveness against *C. albicans* strains and the colloidal stability of loaded nanoparticles, it can be assured that acylated nanoparticles fulfil all needed requirements to be employed as a potential AmB drug delivery system.

**Supplementary Materials:** The following are available online at <https://www.mdpi.com/article/10.3390/colloids6040065/s1>, Figure S1: FT-IR spectra expansion in the range of  $3100\text{--}2750\text{ cm}^{-1}$  for (A) CG; (B) CGAc; (C) CGProp, (D) CGBut.



**Author Contributions:** Conceptualization, A.R.R., R.C.M.d.P. and F.M.G.; methodology, J.D.B.M.-F., A.J.A., J.P.A.F., and R.O.S.F.; validation, A.R.R. and R.C.M.d.P.; formal analysis, A.R.R., J.F.S.M., S.A.N.M.S., J.G.V.-N., and J.S.S.; investigation, A.R.R., J.F.S.M., S.A.N.M.S. and J.G.V.-N.; data curation, R.C.M.d.P. and H.C.B.P.; writing—original draft preparation, A.R.R. and R.C.M.d.P.; writing—review and editing, R.C.M.d.P., H.C.B.P., J.P.A.F. and F.M.G.; supervision, R.C.M.d.P.; project administration; R.C.M.d.P. and J.P.A.F.; funding acquisition, R.C.M.d.P. and J.P.A.F. All authors have read and agreed to the published version of the manuscript.

**Funding:** This research was funded by CNPq (grant 408511/2016-8), CAPES (PROEX 23038.000509/2020-82). National Institute of Science and Technology—INCT BioNat, (CNPQ grant # 465637/2014-0, FAPESP grant # 2014/50926-0), National Institute of Science and Technology—INCT-INOMAT (CNPQ grant # 465452\_2014-0 Brazil).

**Data Availability Statement:** Not applicable.

**Acknowledgments:** The authors gratefully acknowledge CENAUREM for NMR analyzes.

**Conflicts of Interest:** Authors declare no conflict of interest.

## References

- Rubey, K.M.; Brenner, J.S. Nanomedicine to fight infectious disease. *Adv. Drug Deliv. Rev.* **2021**, *179*, 113996. [[CrossRef](#)] [[PubMed](#)]
- Prasanna, P.; Kumar, P.; Kumar, S.; Rajana, V.K.; Kant, V.; Prasad, R.S.; Mohan, U.; Mandal, D. Current status of nanoscale drug delivery and the future of nano-vaccine development for leishmaniasis—A review. *Biomed. Pharmacother.* **2021**, *141*, 111920. [[CrossRef](#)] [[PubMed](#)]
- Maltezou, H.C. Drug resistance in visceral leishmaniasis. *J. Biomed. Biotechnol.* **2010**, *2010*, 617521. [[CrossRef](#)] [[PubMed](#)]
- Caldeira, L.R.; Fernandes, F.R.; Costa, D.F.; Frézard, F.; Afonso, L.C.C.; Ferreira, L.A.M. Nanoemulsions loaded with amphotericin B: A new approach for the treatment of leishmaniasis. *Eur. J. Pharm. Sci.* **2015**, *70*, 125–131. [[CrossRef](#)]
- Liu, Y.C.; Han, Y.; Fang, T.; Cheng, S.M.; Hu, X.Y.; Song, L.J.; Shen, H.; Dong, H.Q.; Jiang, Y.Y.; An, M.M. Turning weakness into strength: Albumin nanoparticle-redirected amphotericin B biodistribution for reducing nephrotoxicity and enhancing antifungal activity. *J. Control. Release* **2020**, *324*, 657–668. [[CrossRef](#)]
- Gedda, M.R.; Madhukar, P.; Shukla, A.; Mudavath, S.L.; Srivastava, O.N.; Singh, O.P.; Sundar, S. Nanodiagnostics in leishmaniasis: A new frontiers for early elimination. *Rev. Nanomed. Nanobiotechnol.* **2020**, *13*, e1675. [[CrossRef](#)]
- Saqib, M.; Bhatti, A.S.A.; Ahmad, N.M.; Ahmed, N.; Shahnaz, G.; Lebaz, N.; Elaissari, A. Amphotericin B Loaded Polymeric Nanoparticles for Treatment of Leishmania Infections. *J. Nanomater.* **2020**, *10*, 1152. [[CrossRef](#)]
- Richter, A.R.; Carneiro, M.J.M.; Sousa, N.A.; Pinto, V.P.T.; Freire, R.S.; de Sousa, J.S.; Mendes, F.S.; Fontenelle, R.O.S.; Feitosa, J.P.A.; Paula, H.C.B.; et al. Self-assembling cashew gum-graft-poly lactide copolymer nanoparticles as a potential amphotericin B delivery matrix. *Int. J. Biol. Macromol.* **2020**, *152*, 492–502. [[CrossRef](#)]
- Ariaga, K.; Nishikawa, M.; Mori, T.; Takeya, J.; Shrestha, L.K.; Hill, J.P. Self-assembly as a key player for materials nanoarchitectonics. *Sci. Technol. Adv. Mater.* **2019**, *20*, 51–95. [[CrossRef](#)]
- Yadav, S.; Sharma, A.K.; Kumar, P. Nanoscale self-assembly for therapeutic drug loading for pH-triggered drug delivery. *Biomacromolecules* **2020**, *15*, 524–532. [[CrossRef](#)]
- Fan, Y.; Liu, Y.; Wu, Y.; Dai, F.; Yuan, M.; Bai, Y.; Deng, H. Natural polysaccharide based self-assembled nanoparticles for biomedical applications—A review. *Int. J. Biol. Macromol.* **2021**, *192*, 1240–1255. [[CrossRef](#)] [[PubMed](#)]
- Lemarchand, C.; Gref, R.; Couvreur, P. Polysaccharide-decorated nanoparticles. *Eur. J. Pharm. Biopharm.* **2004**, *58*, 327–341. [[CrossRef](#)] [[PubMed](#)]
- de Paula, R.C.M.; Heatley, F.; Budd, P.M. Characterization of *Anacardium occidentale* exudate polysaccharide. *Polym. Int.* **1998**, *45*, 27–35. [[CrossRef](#)]
- Menestrina, J.M.; Iacomini, M.; Jones, C.; Gorin, P.A.J. Similarity of monosaccharide, oligosaccharide, and polysaccharide structure in gum from *Anacardium occidentale*. *Phytochemistry* **1998**, *47*, 715–721. [[CrossRef](#)]
- Ribeiro, A.J.; Souza, F.R.L.; Bezerra, J.M.N.A.; Oliveira, C.; Nadvorny, D.; Soares, M.F.R.; Nunes, L.C.C.; Silva-Filho, E.C.; Veiga, F.; Sobrinho, J.L.S. Gums' based delivery systems: Review on cashew gum and its derivatives. *Carbohydr. Polym.* **2016**, *147*, 188–200. [[CrossRef](#)]
- Kumar, A.; Moin, A.; Shruthi, R.; Ahmed, A.; Shivakumar, H.G. Cashew Gum: A Versatile Hydrophilic Polymer: A Review. *Curr. Drug Ther.* **2012**, *7*, 2–12. [[CrossRef](#)]
- Nayak, A.K.; Ansari, M.T.; Sami, F.; Bera, H.; Hasnain, M.S. Cashew gum in drug delivery applications. In *Natural Polysaccharides in Drug Delivery and Biomedical Applications*; Hasnain, M.S., Nayak, A.K., Eds.; Academic Press: Cambridge, MA, USA, 2019; pp. 263–283.
- Dueramae, I.; Yoneyama, M.; Shinyashiki; Yagihara, N.; Kita, S.R. Self-assembly of acetylated dextran with various acetylation degrees in aqueous solutions: Studied by light scattering. *Carbohydr. Polym.* **2017**, *159*, 171–177. [[CrossRef](#)]
- Najafi, S.H.M.; Baghaie, M.; Ashori, A. Preparation and characterization of acetylated starch nanoparticles as drug carrier: Ciprofloxacin as a model. *Int. J. Biol. Macromol.* **2016**, *87*, 48–54. [[CrossRef](#)]

20. Ribeiro, A.C.; Rocha, A.; Soares, R.M.D.; Fonseca, L.P.; da Silveira, N.P. Synthesis and characterization of acetylated amylose and development of inclusion complexes with rifampicin. *Carbohydr. Polym.* **2017**, *157*, 267–274. [[CrossRef](#)]
21. Xie, J.H.; Zhang, F.; Wang, Z.J.; Shen, M.Y.; Nie, S.P.; Xie, M.Y. Preparation, characterization and antioxidant activities of acetylated polysaccharides from *Cyclocarya paliurus* leaves. *Carbohydr. Polym.* **2015**, *133*, 596–604. [[CrossRef](#)]
22. Pitombeira, N.A.O.; Veras Neto, J.G.; Silva, D.A.; Feitosa, J.P.A.; Paula, H.C.B.; de Paula, R.C.M. Self-assembled nanoparticles of acetylated cashew gum: Characterization and evaluation as potential drug carrier. *Carbohydr. Polym.* **2015**, *117*, 610–615. [[CrossRef](#)] [[PubMed](#)]
23. Dias, S.F.L.; Nogueira, S.S.; Dourado, F.F.; Guimaraes, M.A.; Pitombeira, N.A.O.; Gobbo, G.G.; Primo, F.L.; de Paula, R.C.M.; Feitosa, J.P.A.; Tedesco, A.C.; et al. Acetylated cashew gum-based nanoparticles for transdermal delivery of diclofenac diethyl amine. *Carbohydr. Polym.* **2016**, *143*, 254–261. [[CrossRef](#)] [[PubMed](#)]
24. Lima, M.R.; Paula, H.C.B.; Abreu, F.O.M.; da Silva, R.B.C.; Sombra, F.M.; de Paula, R.C.M. Hydrophobization of cashew gum by acetylation mechanism and amphotericin B encapsulation. *Int. J. Biol. Macromol.* **2018**, *108*, 523–530. [[CrossRef](#)] [[PubMed](#)]
25. Rodrigues, J.D.; de Araújo, A.R.; Pitombeira, N.A.; Placido, A.; de Almeida, M.P.; Veras, L.M.C.; Delerue-Matos, C.; Lima, F.C.D.A.; Batagin Neto, A.; de Paula, R.C.M.; et al. Acetylated cashew gum-based nanoparticles for the incorporation of alkaloid epiisopiloturine. *Int. J. Biol. Macromol.* **2019**, *128*, 965–972. [[CrossRef](#)] [[PubMed](#)]
26. Silva, E.L.; Oliveira, A.C.J.; Patriota, Y.B.C.; Ribeiro, A.J.; Veiga, F.; Sobrinho, F. Solvent-free synthesis of acetylated cashew gum for oral delivery system of insulin. *Carbohydr. Polym.* **2019**, *207*, 601–608. [[CrossRef](#)]
27. Biswas, A.; Cheng, H.N.; Kim, S.; Albes, C.R.; Furtadi, R.F. Hydrophobic modification of cashew gum with alkenyl succinic anhydride. *Polymers* **2020**, *12*, 514. [[CrossRef](#)]
28. Oliveira, A.C.J.; Chaves, L.P.; Ribeiro, F.O.S.; Lima, L.R.M.; Oliveira, T.C.; García-Villén, F.; Viseras, C.; de Paula, R.C.M.; Rolim-Neto, P.J.; Hallwass, F.; et al. Microwave-initiated rapid synthesis of phthalated cashew gum for drug delivery systems. *Carbohydr. Polym.* **2021**, *254*, 117226. [[CrossRef](#)]
29. Rodrigues, J.F.; de Paula, R.C.M.; Costa, S.M.O. Métodos de Isolamento de Gomas Naturais: Comparação Através da Goma do Cajueiro (*Anacardium occidentale* L). *Polímeros Ciência Tecnol.* **1993**, *3*, 31–36.
30. Motozato, Y.; Ihara, H.; Tomoda, T.; Hirayama, C. Preparation and gel permeation chromatographic properties of pullulan spheres. *J. Chromatogr.* **1986**, *355*, 434–437. [[CrossRef](#)]
31. Sánchez-Rivera, M.M.; Flores-Ramírez, I.; Zamudio-Flores, P.B.; Gonzalez-Soto, R.A.; Rodríguez-Ambríz, S.L.; Bello-Pérez, L.A. Acetylation of banana (*Musa paradisiaca* L.) and maize (*Zea mays* L.) starches using a microwave heating procedure and iodine as catalyst: Partial characterization. *Starch/Staerke* **2010**, *62*, 155–164. [[CrossRef](#)]
32. Garg, S.; Jana, A.K. Characterization and evaluation of acylated starch with different acyl groups and degrees of substitution. *Carbohydr. Polym.* **2011**, *83*, 1623–1630. [[CrossRef](#)]
33. Malvern. Zetasizer Nano Series. Malvern Instrument SZ User Manual. Dynamic Light Scattering DLS | Malvern Panalytical. Available online: <https://www.malvernpanalytical.com/en/products/technology/light-scattering/dynamic-light-scattering> (accessed on 1 October 2022).
34. Barwicz, J.; Christian, S.; Gruda, I. Effects of the aggregation state of amphotericin B on its toxicity to mice. *Antimicrob. Agents Chemother.* **1992**, *36*, 2310–2315. [[CrossRef](#)] [[PubMed](#)]
35. Clinical and Laboratory Standart Institute. *Reference Method for Broth Dilution Antifungal Susceptibility Testing of Yeast*, 3rd ed.; Approved Standard M27-A3; CSLI: Wayne, PA, USA, 2008.
36. Mosmann, T. Rapid colorimetric assay for cellular growth and survival: Application to proliferation and cytotoxicity assays. *J. Immunol. Methods* **1983**, *65*, 55–63. [[CrossRef](#)]
37. Sombra, F.M.; Richter, A.R.; de Araújo, A.R.; Ribeiro, F.O.S.; Mendes, J.F.S.; Fontenelle, R.O.S.; Silva, D.A.; Paula, H.C.B.; Feitosa, J.P.A.; Goycoolea, F.M.; et al. Nanocapsules of *Sterculia striata* acetylated polysaccharide as a potential monomeric amphotericin B delivery matrix. *Int. J. Biol. Macromol.* **2019**, *130*, 655–663. [[CrossRef](#)] [[PubMed](#)]
38. Sombra, F.M.; Richter, A.R.; de Araújo, A.R.; Ribeiro, F.O.S.; Mendes, J.F.S.; Fontenelle, R.O.S.; Silva, D.A.; Paula, H.C.B.; Feitosa, J.P.A.; Goycoolea, F.M.; et al. Development of amphotericin B-loaded propionate *Sterculia striata* polysaccharide nanocarrier. *Int. J. Biol. Macromol.* **2020**, *146*, 1133–1144. [[CrossRef](#)]
39. Cunha, P.L.R.; Maciel, J.S.; Sierakowski, M.R.; de Paula, R.C.M.; Feitosa, J.P.A. Oxidation of cashew tree gum exudate polysaccharide with TEMPO reagent. *J. Braz. Chem. Soc.* **2007**, *18*, 85–92. [[CrossRef](#)]
40. Silva, D.A.; de Paula, R.C.M.; Feitosa, J.P.A.; de Brito, A.C.F.; Maciel, J.S.; Paula, H.C.B. Carboxymethylation of cashew tree exudate polysaccharide. *Carbohydr. Polym.* **2004**, *58*, 163–171. [[CrossRef](#)]
41. Moura Neto, E.; Maciel, J.S.M.; Cunha, P.L.R.; de Paula, R.C.M.; Feitosa, J.P.A. Preparation and characterization of a chemically sulfated cashew gum polysaccharide. *J. Braz. Chem. Soc.* **2011**, *22*, 1953–1960. [[CrossRef](#)]
42. Kemas, C.U.; Ngwuluka, N.C.; Ochekepe, N.A.; Nep, E.I. Starch-based xerogels: Effect of acetylation on Physicochemical and rheological properties. *Int. J. Biol. Macromol.* **2017**, *98*, 94–102. [[CrossRef](#)]
43. Niu, B.; Shao, P.; Chen, H.J.; Sun, P.L. Structural and physicochemical characterization of novel hydrophobic packaging films based on pullulan derivatives for fruits preservation. *Carbohydr. Polym.* **2019**, *208*, 276–284. [[CrossRef](#)]
44. Zhu, X.; Zhang, X.; Gao, X.; Meng, X.; Yi, Y. Synthesis and Characterization of Inulin Butyrate Ester, and Evaluation of Its Antioxidant Activity and in Vitro Effect on SCFA Production. *Starch/Staerke* **2020**, *72*, 1900323. [[CrossRef](#)]

45. Patel, V.R.; Agrawal, Y.K. Nanosuspension: An approach to enhance solubility of drugs. *J. Adv. Pharm. Technol. Res.* **2011**, *2*, 81–87. [[CrossRef](#)] [[PubMed](#)]
46. Bhattacharjee, S. DLS end zeta—What they are and what they are not? *J. Control. Release* **2016**, *235*, 337–351. [[CrossRef](#)] [[PubMed](#)]
47. Di Martino, A.; Sedlarik, V. Amphiphilic chitosan-grafted-functionalized polylactic acid based nanoparticles as a delivery system for doxorubicin and temozolomide co-therapy. *Int. J. Pharm.* **2014**, *474*, 134–145. [[CrossRef](#)] [[PubMed](#)]
48. Brasili, F.; Capocefalo, A.; Palmieri, D.; Capitano, F.; Chiessi, E.; Paradossi, G.; Bordi, F.; Domenici, F. Assembling patchy plasmonic nanoparticles with aggregation-dependent antibacterial activity. *J. Colloid Interface Sci.* **2020**, *580*, 419–428. [[CrossRef](#)]
49. Sennato, S.; Truzzolillo, D.; Bordi, F. Aggregation and stability of polyelectrolyte-decorated liposome complexes in water-salt media. *Soft Matter* **2012**, *8*, 9384–9395. [[CrossRef](#)]
50. Hierrezuelo, J.; Sadeghpour, A.; Szilagyi, I.; Vaccaro, A.; Borkovec, M. Electrostatic stabilization of charged colloidal particles with adsorbed polyelectrolytes of opposite charge. *Langmuir* **2010**, *26*, 15109–15111. [[CrossRef](#)]
51. Kouchakzadeh, H.; Shojaosadati, S.A.; Maghsoudi, A.; Farahani, E.V. Optimization of PEGylation conditions for BSA nanoparticles using response surface methodology. *Aaps Pharmscitech* **2010**, *11*, 1206–1211. [[CrossRef](#)]
52. Adair, J.H.; Suvaci, E.; Sindel, J. Surface and Colloid Chemistry. In *Encyclopedia of Materials: Science and Technology*; Buschow, R.W., Cahn, M.C., Flemings, B., Ilshner, E.J., Kramer, S., Mahajan, P., Eds.; Elsevier: Amsterdam, The Netherlands, 2001; pp. 1–10. [[CrossRef](#)]
53. Tancrede, P.; Barwicz, J.; Jutras, S.; Gruda, I. The effect of surfactants on the aggregation state of amphotericin B. *Biochim. Biophys. Acta.* **1990**, *1030*, 289–295. [[CrossRef](#)]
54. Casa, D.M.; Carraro, T.C.; Camargo, L.E.; Dalmolin, L.F.; Khalil, N.M.; Mainardes, R.M. Poly(L-lactide) nanoparticles reduce amphotericin B cytotoxicity and maintain its in vitro antifungal activity. *J. Nanosci. Nanotechnol.* **2015**, *15*, 848–854. [[CrossRef](#)]
55. Wang, Y.; Ke, X.; Voo, Z.X.; Yap, S.S.L.; Yang, C.; Gao, S.; Liu, S.; Venkataraman, S.; Khara, S.J.; Yang, Y.Y.; et al. Biodegradable functional polycarbonate micelles for controlled release of amphotericin B. *Acta Biomater.* **2016**, *46*, 211–220. [[CrossRef](#)] [[PubMed](#)]
56. Bolard, J.; Seigneuret, M.; Boudet, G. Interaction between phospholipid bilayer membranes and the polyene antibiotic amphotericin b lipid state and cholesterol content dependence. *Biochim. Biophys. Acta.* **1980**, *599*, 280–293. [[CrossRef](#)]
57. Song, Z.M.; Wen, Y.; Deng, P.Z.; Teng, F.F.; Zhou, F.L.; Xu, H.M.; Feng, S.J.; Zhu, L.; Feng, R.L. Linolenic acid-modified methoxy poly (ethylene glycol)-oligochitosan conjugate micelles for encapsulation of amphotericin B. *Carbohydr. Polym.* **2019**, *205*, 571–580. [[CrossRef](#)] [[PubMed](#)]
58. Mullen, A.B.; Carter, K.C.; Baillie, A.J. Comparison of the efficacies of various formulations of amphotericin B against murine visceral leishmaniasis. *Antimicrob. Agents Chemother.* **1997**, *41*, 2089–2092. [[CrossRef](#)]
59. Tiyaboonchai, W.; Limpeanchob, N. Formulation and characterization of amphotericin B-chitosan-dextran sulfate nanoparticles. *Int. J. Pharm.* **2007**, *329*, 142–149. [[CrossRef](#)]
60. Gilani, K.; Moazeni, E.; Ramezanli, T.; Amini, M.; Fazeli, M.R.; Jamalifar, H. Development of respirable nanomicelle carriers for delivery of amphotericin B by jet nebulization. *J. Pharma. Sci.* **2011**, *100*, 252–259. [[CrossRef](#)]
61. Imran, M.; Shah, M.R.; Ullah, F.; Ullah, S.; Elhissi, A.M.A.; Nawaz, W.; Ahmad, F.; Sadiq, A.; Ali, I. Sugar-based novel niosomal nanocarrier system for enhanced oral bioavailability of levofloxacin. *Drug Deliv.* **2016**, *23*, 3653–3664. [[CrossRef](#)]
62. Italia, J.L.; Yahya, M.M.; Singh, D.; Kumar, M.N.V.R. Biodegradable nanoparticles improve oral bioavailability of amphotericin B and show reduced nephrotoxicity compared to intravenous fungizone<sup>®</sup>. *Pharm. Res.* **2009**, *26*, 1324–1331. [[CrossRef](#)]
63. Krishnan, R.A.; Pant, T.; Sankaranarayan, S.; Stenberg, J.; Jain, R.; Dandekar, P. Protective nature of low molecular weight chitosan in a chitosan–Amphotericin B nanocomplex—A physicochemical study. *Mater. Sci. Eng. C* **2018**, *93*, 472–482. [[CrossRef](#)]
64. Zeng, L.; An, L.; Wu, X. Modeling drug-carrier interaction in the drug release from nanocarriers. *J. Drug. Deliv.* **2011**, *2011*, 370308. [[CrossRef](#)]
65. Chronopoulou, L.; Domenici, F.; Giantulli, S.; Brasili, F.; D’Errico, C.; Tsaoili, G.; Tortorella, E.; Bordi, F.; Morrone, S.; Palocci, C.; et al. PLGA based particles as “drug reservoir” for antitumor drug delivery: Characterization and cytotoxicity studies. *Colloids Surf. B.* **2019**, *180*, 495–502. [[CrossRef](#)] [[PubMed](#)]
66. Mutlu-Agardan, N.B.; Yilmaz, S.; Onurdag, F.K.; Celebi, N. Development of effective AnB/AmB- $\alpha$ CD complex double loaded liposomes using a factorial design for systemic fungal infection treatment. *J. Liposome. Res.* **2021**, *31*, 177–188. [[CrossRef](#)] [[PubMed](#)]